Inter-frequency all-optical transfer of structured light information in Rb vapor based on spatial cross-phase modulation

Cite as: Appl. Phys. Lett. **126**, 151104 (2025); doi: 10.1063/5.0256568
Submitted: 6 January 2025 · Accepted: 4 April 2025 ·
Published Online: 15 April 2025

Junfei Chen,[1] Zhiping Wang,[1,a)] Hamid R. Hamedi,[2,b)] and Benli Yu[1]

AFFILIATIONS

[1]National Key Laboratory of Opto-Electronic Information Acquisition and Protection Technology, Information Materials and Intelligent Sensing Laboratory of Anhui Province, and Key Laboratory of Opto-Electronic Information Acquisition and Manipulation of Ministry of Education, Anhui University, Hefei 230601, China
[2]Institute of Theoretical Physics and Astronomy, Vilnius University, Saulėtekio 3, Vilnius LT-10222, Lithuania

[a)]Author to whom correspondence should be addressed: wzp@ahu.edu.cn
[b)]Electronic mail: hamid.hamedi@tfai.vu.lt

ABSTRACT

High-dimensional all-optical information transfer facilitates large-capacity, high-speed, and energy-efficient optical communication, playing a pivotal role in advancing modern photonic technologies. Here, we demonstrate the all-optical transfer of structured information between two beams with different frequencies via spatial cross-phase modulation in a hot ^{85}Rb vapor. A high-power pump beam, characterized by a structured light, induces a refractive index change in the rubidium vapor. A low-power, initially Gaussian probe beam counter-propagates through the rubidium vapor cell, undergoing a nonlinear phase shift induced by the pump beam. This enables the transfer of the spatial characteristics imprinted by the pump beam onto the probe beam with maximum structural integrity and similarity. The spatial evolution of the transverse intensity of the probe beam vs frequency detunings of the pump and probe beams, pump beam power, and cell temperature is studied. We have further shown that the structural similarity can be manipulated by changing the pump beam power and temperature of the vapor cell. Our findings may reveal a way to manipulate light fields, offering potential applications in optical communication, all-optical data processing, and advanced photonic devices.

Cross-phase modulation (XPM), as one of the optical Kerr effects, plays an important role in quantum nonlinear optics.[1] Different from self-phase modulation (SPM),[2,3] XPM typically refers to the intensity variation of one light wave inducing a phase change of another light wave when two light waves of different wavelengths propagate through a nonlinear medium.[4–6] Owing to the practical advantages for all-optical information conversion,[7] XPM has been widely applied in various fields, such as optical communication,[8] all-optical information conversion,[9–12] quantum entanglement,[13] non-reciprocal devices[14] the generation of Bessel-like beams.[15] However, the structured light waves have not yet been explored in hot atoms to realize all-optical information conversion based on XPM.

In recent decades, structured light waves have also gained much interest, partially due to their unique spatial beam structures with tailored amplitude and phasefronts.[16–19] One type of structured light waves is a vortex beam carrying orbital angular momentum (OAM).[20,21] Unlike the conventional Gaussian beam, the structured light wave generally refers to an optical beam with a tailored spatial amplitude/phase distribution and corresponding unique properties, which has led to many remarkable applications in optical micro-processing,[22,23] far-field super-resolution imaging,[24] optical communication,[25] and optical micro-manipulation.[26–28] Moreover, by adjusting the polarization state of the structured light,[29–32] the modulation instability can also be effectively controlled.

In this work, we investigate the all-optical transfer of structured information between two different frequency beams using XPM in hot atoms. The pump beam is a superposition mode coherently superposed by two Laguerre–Gaussian (LG) beam modes, creating a structured-beam profile, which induces a change in the nonlinear refractive index of the rubidium vapor. When the Gaussian probe beam passes through the rubidium vapor cell, it acquires the nonlinear phase shift information from the pump beam, resulting in the transfer of structured information. The spatial evolution of the transverse intensity of the probe beam vs frequency detunings of the pump and probe beams, pump beam power, and cell temperature is studied. We have further shown that the structural similarity can be manipulated by changing the pump beam power and temperature of the vapor cell. The present study may provide a useful tool for transferring various types of structured light beams.

The pump beam after passing the Q-plate is a Laguerre–Gaussian (LG) mode, the electric field distribution in cylindrical coordinates (r, ϕ, z) are given by[33]

$$\mathbf{E}_{p\ell}(r, \phi, z) = \mathbf{E}\exp(i\ell\phi)\hat{\mathbf{e}}, \tag{1}$$

where $\mathbf{E}(r,z) = E_0\left(\frac{\sqrt{2}r}{w(z)}\right)^{|\ell|} L_p^{|\ell|}\left(\frac{2r^2}{w^2(z)}\right)\exp\left(-\frac{r^2}{w^2(z)}\right)\exp\left\{-i\left[kz+\frac{kr^2}{2R(z)}\right.\right.$ $\left.\left.-(2p+|\ell|+1)\arctan\left(\frac{z}{z_R}\right)\right]\right\}$, E_0 is the amplitude of the electric field, r is the radial distance from the beam axis, ϕ is the azimuthal angle, z is the longitudinal coordinate, $w(z) = w_0\sqrt{1+(z_R/z)^2}$ is the beam radius at position z, w_0 is the beam waist, $z_R = \pi w_0^2/\lambda$ is the Rayleigh range, λ is the wavelength, $k = 2\pi/\lambda$ is the wave vector, $R(z) = z\left[1+(z_R/z)^2\right]$ is the radius of curvature of the wavefronts, $L_p^{|\ell|}$ is the associated Laguerre polynomial, p is the radial index, ℓ is the azimuthal index (also known as the topological charge), and $\hat{\mathbf{e}}$ is the polarization vector.

When the pump beam is reflected by the polarizing beam splitter (PBS_1), the pump beam becomes a y-polarized superposition mode, which is coherently superposed by two LG beam modes with equal but opposite OAM, thus creating a structured-beam profile given by

$$\mathbf{E}_y = \mathbf{E}(r,z)[\exp(i\ell\phi)+\exp(-i\ell\phi)]\hat{\mathbf{e}}_y, \tag{2}$$

where $\hat{\mathbf{e}}_y$ is the y axis polarization vector.

The electric field distribution of the probe beam propagating along the z axis can be described as[34]

$$E(r,z_0) = E(0,z_0)\exp\left(-\frac{ikr^2}{2R(z)}\right)\exp\left(-\frac{r^2}{\omega_p^2}\right), \tag{3}$$

where r is the radial coordinate, z_0 is the position coordinate of the medium entrance plane, and $E(0, z_0)$ represents the electric field of the entrance plane center of the medium. $k = 2\pi/\lambda$ describes the wave vector, and $R(z) = z + z_R^2/z$ is the curvature radius of the wavefront. The spot size of the beam at a given z-position is given by $\omega_p = \omega_0\left(1+z^2/z_R^2\right)^{1/2}$, and here ω_0 is the waist radius and $z_R = \pi\omega_0^2/\lambda$ is the Rayleigh length.

When the strong pump beam passes through the atomic medium with an effective interaction length of L_{eff}, the Kerr nonlinear effect induced by the spatial XPM, which makes the refractive index of medium is spatially modulated. As the weak probe beam passes through the medium, which acquires a nonlinear phase shift influenced by the pump beam, it effectively transfers the structured information of the pump to the probe beam.[15] Given the significant intensity difference between the pump beam I_1 and the probe beam I_2, the pump beam plays a dominant role in the spatial XPM process. Therefore, the nonlinear phase shift of the probe laser beam is expressed as[35]

$$\phi_{probe}(r) = \Delta\phi_{probe}\exp\left(-\frac{2r^2}{\omega_p^2}\right), \tag{4}$$

where $\Delta\phi_{probe}(r) = 2kn_2L_{eff}I_1$ represents the peak nonlinear phase of the probe beam, which is twice that of the pump beam $\Delta\phi_{pump}(r) = kn_2L_{eff}I_1$. Here, n_2 is the nonlinear refractive index of the medium, given by[15]

$$n_2 \propto \frac{\mu_{12}^4 N}{2c\varepsilon_0^2 h^3\Delta^3}, \tag{5}$$

where μ_{12} denotes the dipole matrix element, N is the atomic number density, and Δ is the frequency detuning. Clearly, the nonlinear phase shift can be significantly adjusted by the intensity of the pump laser, the atomic number density, and the frequency detuning. Note that the nonlinear refractive index n_2 is directly proportional to the μ_{12}, which depends on the spatial polarization state of the pump beam. The spatially varying polarization superposition mode ($\mathbf{E}_y$) induces an azimuthal modulation of the atomic dipole coupling strength (μ_{12}), which directly governs the nonlinear refractive index (n_2). Therefore, by engineering the spatial polarization state of the structured pump beam, one can tailor the nonlinear refractive index n_2 to achieve the desired transfer of structured light information in Rb vapor based on spatial XPM, and the spatial polarization state of the pump beam is a critical degree of freedom for controlling the overall XPM.

Structural similarity (SSIM) is an index used to measure the similarity between two images. It evaluates the similarity by comparing three main components: brightness, contrast, and structure. The calculation formula of SSIM is as follows:[36]

$$\mathrm{SSIM} = [l(x,y)]^{\alpha}\cdot[c(x,y)]^{\beta}\cdot[s(x,y)]^{\gamma}, \tag{6}$$

where x and y are the corresponding regions of the two images being compared. In Eq. (6), $l(x,y) = \frac{2\mu_x\mu_y+C_1}{\mu_x^2+\mu_y^2+C_1}$ represents the brightness comparison function, $c(x,y) = \frac{2\sigma_x\sigma_y+C_2}{\sigma_x^2+\sigma_y^2+C_2}$ is the contrast comparison

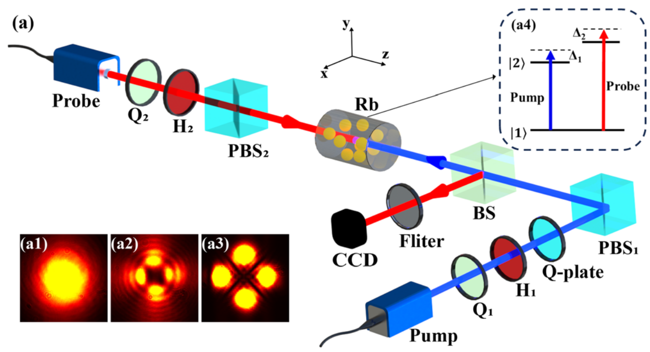

FIG. 1. Detailed experimental setup. (a1) The intensity profile of the probe beam before entering the atom cell. The intensity profile of the pump beam (a2) before and (a3) after passing through the atom cell. (a4) The three-level atomic system. Q_i $(i = 1, 2)$, quarter-wave plate; H_j $(j = 1, 2, 3)$, half-wave plate; PBS_k $(k = 1, 2)$, polarizing beam splitter; BS, optical splitter; Q-plate, spiral phase plate; Rb, a normal Rb gas cell (length 10 cm) without buffer gas; CCD, charge-coupled camera; Filter, bandpass filter with a center wavelength of 780.8 nm (bandwidth 10 nm).

function, $s(x,y)=\frac{\sigma_{xy}+C_3}{\sigma_x\sigma_y+C_3}$ shows the structure comparison function. Here, μ_x and μ_y are the average values of x and y in the image region, respectively; σ_x and σ_y are the standard deviations of the image region x and y, respectively. σ_{xy} is the covariance between regions x and y. The constants C_1, C_2, and C_3 are small constants added to avoid zeroing errors, usually set according to the dynamic range of the image. When calculating, one sets $\alpha=\beta=\gamma=1$ and $C_3=C_2/2$.

The experimental setup is shown in Fig. 1. The system incorporates a cylindrical rubidium vapor cell fabricated from transparent glass, with precise dimensions of 25 mm in diameter and 100 mm in length. To ensure accurate temperature regulation, the vapor cell is housed in a precision temperature control furnace capable of maintaining thermal stability within $\pm 0.1\,^\circ$C throughout the experimental procedures. The probe beam generated by a tunable diode laser (Toptica DL100, center wavelength 780.78 nm, linewidth 100 kHz) is a Gaussian mode [see Fig. 1(a1)]. It propagates through a polarization beam splitter (PBS_2), transmitting a 100-mm-long natural-abundance Rb vapor cell to a beam splitter (BS) and forming an image reflected by the BS in a charge-coupled device (CCD) camera, which is equipped with a narrowband optical filter (center wavelength 780.8 nm, bandwidth 10 nm). The pump beam (generated by a tunable diode laser, center wavelength 795.53 nm, linewidth 100 kHz) is sent to a Q-plate to generate the LG mode with the topological charge $l=2$, and later reflected by a polarizing beam splitter (PBS_1), which becomes a y-polarized superposition mode. The intensity profiles of the pump beam before and after entering the rubidium vapor cell is shown in Figs. 1(a2) and 1(a3), respectively. A three-level atomic system is shown in Fig. 1(a4), which has one ground state, $|1\rangle$, and two excited states, $|2\rangle$ and $|3\rangle$. The designated states can be chosen as $|1\rangle=|5^2S_{1/2},F=3\rangle$, $|2\rangle=|5^2P_{1/2},F=2\rangle$, and $|3\rangle=|5^2P_{3/2},F=4\rangle$. The probe beam couples to the atomic transition $|1\rangle\leftrightarrow|3\rangle$ with a detuning Δ_2, while the pump beam drives the transition $|1\rangle\leftrightarrow|2\rangle$ with a detuning Δ_1.

Figures 2(a1)–2(a12) display the spatial evolution of the transverse intensity of the probe beam vs different temperatures of the rubidium vapor cell. When temperature is 45 or 50 °C, as shown in Figs. 2(a1) and 2(a2), the intensity profile of the probe beam is blurry. As we change the temperature from 55 to 80 °C, one can see that intensity of the probe beam is increasing and shows a "fan-like" profile [see Figs. 2(a3)–2(a8)]. However, as we further increase the cell temperature, the probe field is remarkably absorbed and nearly disappears when the temperature is 100 °C [see Fig. 2(a12)]. For clarity, we plot the probe beam intensity as a function of temperature of the rubidium vapor cell in Fig. 2(b). From this figure, it is clear that the probe beam intensity initially increases and finally decreases with the increasing temperature, which is in good agreement with the experimental findings in Figs. 2(a1)–2(a12). In fact, we note that an increase in temperature results in an increase in the atomic density of the medium, which leads to more frequent collisions and hence more severe decoherence, thereby resulting in a strong absorption of the probe field. Note that the relationship between the atomic number density N and cell temperature is calculated based on Ref. 37.

For a better understanding of the effect of temperature on the transfer of structured light information, the SSIM vs the temperature of the rubidium vapor cell is depicted in Fig. 2(c). As illustrated in this figure, it is evident that there is a strong relationship between the SSIM and the temperature. The findings reveal that one can achieve the optimized SSIM by adjusting the temperature of the rubidium vapor cell.

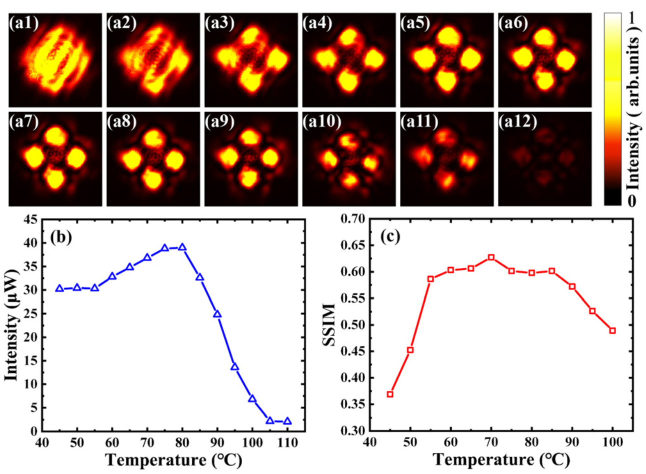

FIG. 2. The spatial evolution of the transverse intensity of the probe beam vs different temperature of the rubidium vapor cell: (a1) 45 °C ($N=9.65\times10^{16}$ m^{-3}), (a2) 50 °C ($N=1.47\times10^{17}$ m^{-3}), (a3) 55 °C ($N=2.27\times10^{17}$ m^{-3}), (a4) 60 °C ($N=3.39\times10^{17}$ m^{-3}), (a5) 65 °C ($N=4.99\times10^{17}$ m^{-3}), (a6) 70 °C ($N=7.27\times10^{17}$ m^{-3}), (a7) 75 °C ($N=1.05\times10^{18}$ m^{-3}), (a8) 80 °C ($N=1.53\times10^{18}$ m^{-3}), (a9) 85 °C ($N=2.19\times10^{18}$ m^{-3}), (a10) 90 °C ($N=3.11\times10^{18}$ m^{-3}), (a11) 95 °C ($N=8.59\times10^{18}$ m^{-3}), and (a12) 100°C ($N=1.19\times10^{19}$ m^{-3}). (b) The probe beam intensity as a function of temperature of the rubidium vapor cell. (c) The SSIM vs the temperature of the rubidium vapor cell. The pump power and probe power are 20 and 0.1 mW, respectively. $\Delta_1=-400$ MHz and $\Delta_2=+1.4$ GHz.

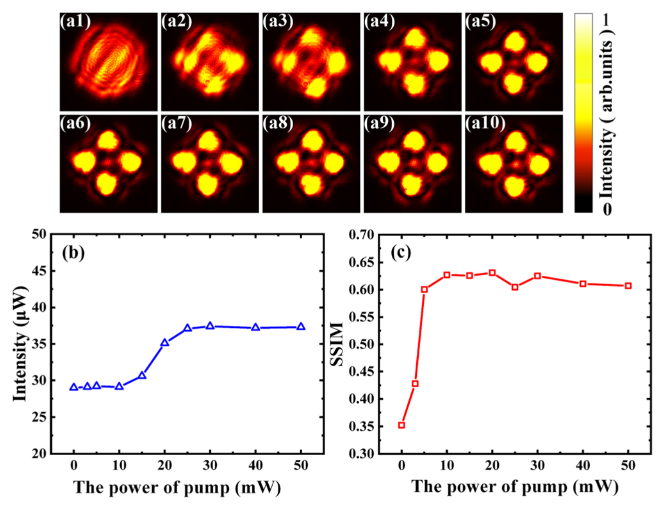

FIG. 3. The spatial evolution of the transverse intensity of the probe beam vs different pump beam power: (a1) 0 mW, (a2) 3 mW, (a3) 5 mW, (a4) 10 mW, (a5) 15 mW, (a6) 20 mW, (a7) 25 mW, (a8) 30 mW, (a9) 40 mW, and (a10) 50 mW. (b) The probe beam intensity as a function of the pump beam power. (c) The SSIM vs the pump beam power. The temperature of the atom cell is 70 °C, $N=7.27\times10^{17}$ m^{-3}, and the other parameters are the same as in Fig. 2.

We now turn to see the influence of the pump beam on the transfer dynamics of the probe beam. The spatial evolution of the transverse intensity of the probe beam vs different pump beam power are shown in Figs. 3(a1)–3(a10). When no pump beam exists or pump beam is weak, as shown in Figs. 3(a1) and 3(a2), the intensity profile of the probe beam remains blurry. When the pump beam power is tuned from 5 to 25 mW, the probe beam is increasing with a fan-like pattern [see Figs. 3(a3)–3(a6)]. As we further increase the pump beam power, there is no significant change in the intensity profile of the probe beam [see Figs. 3(a7)–3(a10)]. For the sake of comparison, we plot probe beam intensity as a function of the pump beam power in Fig. 3(b). From this figure, one can see that probe beam intensity is initially increases but changes limited with further increasing pump beam power. The above results can be qualitatively explained as follows. Once the higher energy states are fully occupied, the rubidium atomic medium cannot absorb more photons from the pump beam, leading to absorption saturation. At this point, further increases in pump beam do not result in the increasing intensity of the probe beam. Also, we show the SSIM vs the pump beam power in Fig. 3(c). As can be clearly noted in this figure, the SSIM is modulated, which is close to 0.62 by an appropriate choice of the pump beam power.

We next study how the pump-beam detuning Δ_1 affects the transverse intensity profile of probe beam. The spatial evolution of the transverse intensity of the probe beam vs different pump-beam detunings are shown in Figs. 4(a1)–4(a12). Clearly, the intensity distributions of the transmitted probe beam is very sensitive to the pump-beam detuning. It is interesting to note in this case that, by appropriately chosen the frequency detuning of pump beam, the nonlinear phase shift can be modulated, so we can see the intensity profile of the probe beam is modulated, as illustrated in Figs. 4(a1)–4(a12).

Finally, we present the spatial evolution of the transverse intensity of the probe beam vs different probe-beam detuning in Figs. 5(a1)–5(a12). It is easy to find from these figures that, at optimal working point of probe-beam detuning, the structured information encoded by the pump beam can effectively transmit to the probe field. However, when the probe-beam detuning $\Delta_2 < +0.8$ GHz or $\Delta_2 > +1.7$ GHz, the probe beam intensity diminishes and its spatial distribution grows less distinct, indicating a reduced efficiency in transferring the structured information of the pump field to the probe beam.

In conclusion, we experimentally demonstrate the all-optical transfer of structured light information between two different frequency beams via cross-phase modulation in hot atoms. When the strong pump beam passes through the atomic medium, the nonlinear effect induced by spatial XPM makes the refractive index of the medium spatially modulated. As the weak probe beam passes through the atoms, it acquires a nonlinear phase shift imprinted by the pump beam, effectively transferring the structured information of the pump to the probe beam. The all-optical transfer can be effectively controlled via the temperature of the atom cell, the optical power of the pump beam, and the frequency detunings of the probe and pump beams. We thus believe that our work may have potential applications in optical communication, quantum sensing, all-optical data processing, and all-optical devices.[38–45]

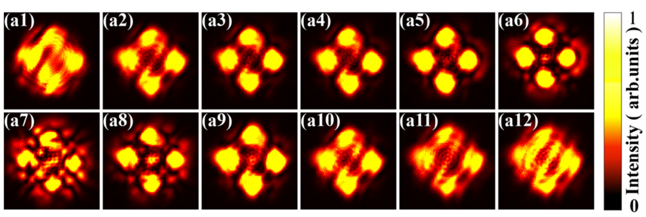

FIG. 4. The spatial evolution of the transverse intensity of the probe beam vs different pump-beam detuning: (a1) -1.2 GHz, (a2) -1 GHz, (a3) -0.8 GHz, (a4) -0.6 GHz, (a5) -0.4 GHz, (a6) -0.2 GHz, (a7) 0, (a8) $+0.2$ GHz, (a9) $+0.4$ GHz, (a10) $+0.6$ GHz, (a11) $+0.8$ GHz, and (a12) $+1$ GHz. The temperature of the atom cell is 70 °C, $N = 7.27 \times 10^{17}$ m^{-3}, and the other parameters are the same as in Fig. 2.

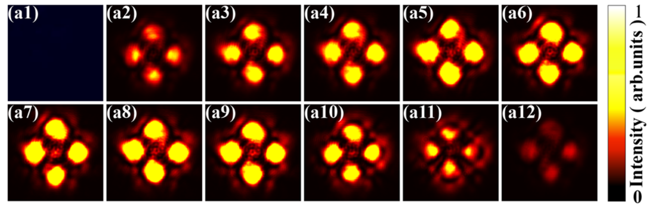

FIG. 5. The spatial evolution of the transverse intensity of the probe beam vs different pump-beam detuning: (a1) $+0.5$ GHz, (a2) $+0.65$ GHz, (a3) $+0.80$ GHz, (a4) $+0.95$ GHz, (a5) $+1.10$ GHz, (a6) $+1.25$ GHz, (a7) $+1.40$ GHz, (a8) $+1.55$ GHz, (a9) $+1.70$ GHz, (a10) $+1.85$ GHz, (a11) $+2.00$ GHz, and (a12) $+2.15$ GHz. The temperature of the atom cell is 70 °C, $N = 7.27 \times 10^{17}$ m^{-3}, and the other parameters are the same as in Fig. 2.

Zhiping Wang gratefully acknowledges the support from the University Natural Science Research Project of Anhui Province (Grant No. 2022AH050115) and the National Natural Science Foundation of China (Grant No. 11674002). Hamid R. Hamedi gratefully acknowledges the support from the Research Council of Lithuania (LMTLT), under Agreement No. S-ITP-24-6.

AUTHOR DECLARATIONS

Conflict of Interest

The authors have no conflicts to disclose.

Author Contributions

Junfei Chen: Data curation (equal); Investigation (equal); Software (equal). **Zhiping Wang:** Funding acquisition (equal); Investigation (equal); Supervision (equal); Writing – original draft (equal); Writing – review & editing (equal). **Hamid R. Hamedi:** Funding acquisition (equal); Writing – review & editing (equal). **Benli Yu:** Writing – review & editing (equal).

DATA AVAILABILITY

The data that support the findings of this study are available from the corresponding author upon reasonable request.

REFERENCES

[1] T. Peyronel, O. Firstenberg, Q.-Y. Liang, S. Hofferberth, A. V. Gorshkov, T. Pohl, M. D. Lukin, and V. Vuletic, "Quantum nonlinear optics with single photons enabled by strongly interacting atoms," Nature **488**, 57–60 (2012).

[2]Q. Zhang, X. Cheng, Y. Zhang, X. Yin, M. Jiang, H. Chen, and J. Bai, "Optical limiting using spatial self-phase modulation in hot atomic sample," Opt. Laser Technol. **88**, 54–60 (2017).
[3]W. Gao, S. Wang, J. Yuan, L. Xiao, S. Jia, and L. Wang, "Identification of orbital angular momentum using atom-based spatial self-phase modulation," Opt. Express **31**, 13528–13535 (2023).
[4]J. D. Swaim, K. N. David, E. M. Knutson, C. Rios, O. Danaci, and R. T. Glasser, "Atomic vapor as a source of tunable, non-gaussian self-reconstructing optical modes," Sci. Rep. **7**, 42311 (2017).
[5]X. Cheng, Q. Zhang, H. Chen, B. He, Z. Ren, Y. Zhang, and J. Bai, "Demonstration of bessel-like beam with variable parameters generated using cross-phase modulation," Opt. Express **25**, 25257–25266 (2017).
[6]Q. Zhang, X. Cheng, B. He, H. Chen, Z. Ren, and J. Bai, "Size-variable dark-hollow beam generation using cross-phase modulation," Opt. Laser Technol. **119**, 105582 (2019).
[7]V. Sasikala and K. Chitra, "All optical switching and associated technologies: A review," J. Opt. **47**, 307–317 (2018).
[8]H. Schmidt and A. Imamoğlu, "High-speed properties of a phase-modulation scheme based on electromagnetically induced transparency," Opt. Lett. **23**, 1007–1009 (1998).
[9]S. Wang, J. Yuan, L. Wang, L. Xiao, and S. Jia, "All-optical information conversion in Rb vapor based on the spatial cross-phase modulation," Opt. Express **30**, 45517–45524 (2022).
[10]A. N. Hassan, M. A. Haddad, A. Behjat, and M. Golestanifar, "Optical nonlinearity and all-optical switching in pumpkin seed oil based on the spatial cross-phase modulation (SXPM) technique," Sci. Rep. **14**, 18158–18158 (2024).
[11]Y. Pan, Z. Lyu, and C. Wang, "All-optical shaping non-conventional beams based on spatial cross-phase modulation," Laser Phys. **31**, 065404 (2021).
[12]Y. Shan, L. Wu, Y. Liao, J. Tang, X. Dai, and Y. Xiang, "A promising nonlinear optical material and its applications for all-optical switching and information converters based on the spatial self-phase modulation (SSPM) effect of $TaSe_2$ nanosheets," J. Mater. Chem. C **7**, 3811–3816 (2019).
[13]M. D. Lukin and A. Imamoğlu, "Nonlinear optics and quantum entanglement of ultraslow single photons," Phys. Rev. Lett. **84**, 1419–1422 (2000).
[14]R. Huang, A. Miranowicz, J.-Q. Liao, F. Nori, and H. Jing, "Nonreciprocal photon blockade," Phys. Rev. Lett. **121**, 153601 (2018).
[15]J. Yuan, X. Wang, L. Wang, L. Xiao, and S. Jia, "Tunable high-order bessel-like beam generation based on cross-phase modulation," Opt. Express **30**, 15978–15985 (2022).
[16]L. Marrucci, C. Manzo, and D. Paparo, "Optical spin-to-orbital angular momentum conversion in inhomogeneous anisotropic media," Phys. Rev. Lett. **96**, 163905 (2006).
[17]N. Radwell, R. D. Hawley, J. B. Goette, and S. Franke-Arnold, "Achromatic vector vortex beams from a glass cone," Nat. Commun. **7**, 10564 (2016).
[18]C. Zheng, J. Li, J. Liu, J. Li, Z. Yue, H. Li, F. Yang, Y. Zhang, Y. Zhang, and J. Yao, "Creating longitudinally varying vector vortex beams with an all-dielectric metasurface," Laser Photonics Rev. **16**, 2200236 (2022).
[19]Z. Liu, Y. Liu, Y. Ke, Y. Liu, W. Shu, H. Luo, and S. Wen, "Generation of arbitrary vector vortex beams on hybrid-order poincare sphere," Photonics Res. **5**, 15–21 (2017).
[20]L. Allen, M. W. Beijersbergen, R. J. C. Spreeuw, and J. P. Woerdman, "Orbital angular momentum of light and the transformation of laguerre-gaussian laser modes," Phys. Rev. A **45**, 8185–8189 (1992).
[21]M. Padgett, J. Courtial, and L. Allen, "Light orbital angular momentum," Phys. Today **57**(5), 35–40 (2004).
[22]C. Hnatovsky, V. Shvedov, W. Krolikowski, and A. Rode, "Revealing local field structure of focused ultrashort pulses," Phys. Rev. Lett. **106**, 123901 (2011).
[23]H. Cheng, P. Li, S. Liu, P. Chen, L. Han, Y. Zhang, W. Hu, and J. Zhao, "Vortex-controlled morphology conversion of microstructures on silicon induced by femtosecond vector vortex beams," Appl. Phys. Lett. **111**, 141901 (2017).
[24]X. Xie, Y. Chen, K. Yang, and J. Zhou, "Harnessing the point-spread function for high-resolution far-field optical microscopy," Phys. Rev. Lett. **113**, 263901 (2014).
[25]G. Milione, T. A. Nguyen, J. Leach, D. A. Nolan, and R. R. Alfano, "Using the nonseparability of vector beams to encode information for optical communication," Opt. Lett. **40**, 4887–4890 (2015).
[26]X.-L. Wang, J. Chen, Y. Li, J. Ding, C.-S. Guo, and H.-T. Wang, "Optical orbital angular momentum from the curl of polarization," Phys. Rev. Lett. **105**, 253602 (2010).
[27]D. Gao, W. Ding, M. Nieto-Vesperinas, X. Ding, M. Rahman, T. Zhang, C. Lim, and C.-W. Qiu, "Optical manipulation from the microscale to the nanoscale: Fundamentals, advances and prospects," Light Sci. Appl. **6**, e17039 (2017).
[28]Z. Yan and N. F. Scherer, "Optical vortex induced rotation of silver nanowires," J. Phys. Chem. Lett. **4**, 2937–2942 (2013).
[29]K. S. Grigoriev, P. S. Ryzhikov, E. B. Cherepetskaya, and V. A. Makarov, "Structure of polarization singularities of a light beam at triple frequency generated in isotropic medium by singularly polarized beam," Opt. Express **25**, 25416–25421 (2017).
[30]J. W. Haus, Z. Mozumder, and Q. Zhan, "Azimuthal modulation instability for a cylindrically polarized wave in a nonlinear kerr medium," Opt. Express **14**, 4757–4764 (2006).
[31]B. Gu, B. Wen, G. Rui, Y. Xue, J. He, Q. Zhan, and Y. Cui, "Nonlinear polarization evolution of hybridly polarized vector beams through isotropic kerr nonlinearities," Opt. Express **24**, 25867–25875 (2016).
[32]M. G. de Oliveira, L. J. Pereira, A. S. Santos, K. Dechoum, A. Bramati, and A. Z. Khoury, "Radial-angular coupling in self-phase-modulation with structured light," Phys. Rev. A **108**, 013503 (2023).
[33]Q. Zhan, "Cylindrical vector beams: From mathematical concepts to applications," Adv. Opt. Photonics **1**, 1–57 (2009).
[34]A. G. Nibu, S. S. Silpa, S. N. Ardra, M. M. Anisha, and D. Ambika, "Effect of viscosity on the far-field diffraction pattern of spatial self-phase modulation," Opt. Appl. **47**, 591–599 (2017).
[35]T. Neupane, B. Tabibi, and F. J. Seo, "Spatial self-phase modulation in WS_2 and MoS_2 atomic layers," Opt. Mater. Express **10**, 831–842 (2020).
[36]Z. Wang, A. Bovik, H. Sheikh, and E. Simoncelli, "Image quality assessment: From error visibility to structural similarity," IEEE Trans. Image Process. **13**, 600–612 (2004).
[37]D. A. Steck, see http://steck.us/alkalidata for "Rubidium 85 d(87 d) line data" (2009).
[38]J. Yuan, W. Yang, M. Jing, H. Zhang, Y. Jiao, W. Li, L. Zhang, L. Xiao, and S. Jia, "Quantum sensing of microwave electric fields based on Rydberg atoms," Rep. Prog. Phys. **86**, 106001 (2023).
[39]J. Yuan, X. Wang, G. Chen, L. Wang, L. Xiao, and S. Jia, "High-fidelity frequency converter in high-dimensional spaces," Laser Photonics Rev. **18**, 2400368 (2024).
[40]H. Kang and Y. Zhu, "Observation of large kerr nonlinearity at low light intensities," Phys. Rev. Lett. **91**, 093601 (2003).
[41]M. Saffman, T. G. Walker, and K. Mølmer, "Quantum information with Rydberg atoms," Rev. Mod. Phys. **82**, 2313–2363 (2010).
[42]S. Wang, J. Yuan, L. Wang, L. Xiao, and S. Jia, "Trans-spectral transfer of spatio-temporal optical ferris wheel with nonlinear wave mixing," Photonics Res. **12**, 2559–2565 (2024).
[43]A. W. Brown, A. Joshi, and M. Xiao, "Controlled steady-state switching in optical bistability," Appl. Phys. Lett. **83**, 1301–1303 (2003).
[44]J. Yuan, H. Zhang, C. Wu, G. Chen, L. Wang, L. Xiao, and S. Jia, "Creation and control of vortex-beam arrays in atomic vapor," Laser Photonics Rev. **17**, 2200667 (2023).
[45]H. Chang, H. Wu, C. Xie, and H. Wang, "Controlled shift of optical bistability hysteresis curve and storage of optical signals in a four-level atomic system," Phys. Rev. Lett. **93**, 213901 (2004).